Published in final edited form as:
Eur J Oral Sci. 2009 December ; 117(6): 625–635. doi:10.1111/j.1600-0722.2009.00690.x.

A new osteopetrosis mutant mouse strain *(ntl)* with odontoma-like proliferations and lack of tooth roots

Xincheng Lu[1,2], **Hector F. Rios**[3], **Baichun Jiang**[4], **Lianping Xing**[5], **Renata Kadlcek**[6], **Edward M. Greenfield**[6], **Guangbin Luo**[1,2], and **Jian Q. Feng**[4]

[1]Department of Genetics, Case Western Reserve University and University Hospitals of Cleveland, Cleveland, OH, USA

[2]Case Comprehensive Cancer Center, Case Western Reserve University and University Hospitals of Cleveland, Cleveland, OH, USA

[3]University of Michigan School of Dentistry 1011 N. University Ann Arbor, MI, USA

[4]Department of Biomedical Sciences, Baylor College of Dentistry, Dallas, TX, USA

[5]Department of Pathology and Laboratory Medicine, University of Rochester Medical Center, Rochester, NY, USA

[6]Department of Orthopaedics, Case Western Reserve University and University Hospitals of Cleveland, Cleveland, OH, USA

Abstract

A new spontaneous mouse mutant (*ntl*) with autosomal-recessive osteopetrosis was characterized. These mice formed tartrate-resistant acid phosphate (TRAP)-positive osteoclasts but their osteoclasts had no ruffled border and did not resorb bone. These mice displayed no tooth eruption or tooth root formation. Adult mutant mice developed odontoma-like proliferations near the proximal ends of the incisors. Intraperitoneal injection of progenitor cells from the liver of 16.5 days postcoitum wild-type embryos into newborn mutants rescued the osteopetrosis phenotype, indicating that the defects were intrinsic to the osteoclasts. Our findings not only provide further support for a critical role of osteoclasts in tooth eruption and tooth root development, but also suggest that the perturbation of the homeostasis of the odontogenic precursors of the incisors is primarily responsible for the development of the odontoma-like proliferations in this osteopetrosis mutant. Genetic mapping has narrowed down the location of the mutant allele to a genetic interval of 3.2 cM on mouse chromosome 17.

Jian Q. Feng, Department of Biomedical Sciences, Baylor College of Dentistry, 3302 Gaston Avenue, Dallas, TX 75246, USA, Telefax: +1–214–3707298, jfeng@bcd.tamhsc.edu. Guangbin Luo, Department of Genetics, Case Comprehensive Cancer Center, Case Western Reserve University and University Hospitals of Cleveland, Cleveland, OH 44106, USA, Telefax: +1–216–3683432, guangbin.luo@case.edu.

Supporting Information

Additional Supporting Information may be found in the online version of this article:

Fig. S1. Whole-mandibular radiographs showing the absence of tooth eruption and root formation in RANK knockout (receptor activator of NF-kappaB) and RANKL knockout mice, two osteopetrosis mouse models.

Please note: Wiley-Blackwell is not responsible for the content or functionality of any supporting materials supplied by the authors. Any queries (other than missing material) should be directed to the corresponding author for the article.

Keywords

odontoma-like proliferations; osteoclast; osteopetrosis; tooth eruption; tooth root formation

Bone homeostasis is maintained primarily by the coordinated activities of two main cellular processes: osteoblast- mediated bone formation; and osteoclast-mediated bone resorption. Perturbation of these coordinated activities can lead to profound alterations in bone mass that have clinical relevance (1, 2). For example, osteoporosis is a common cause of vertebral and compression fractures among the elderly. In addition, rare disorders of increased bone mass caused by the absence or dysfunction of osteoclasts, namely osteopetrosis, can cause death during childhood as a result of ablation of the bone marrow space and skeletal abnormalities caused by the absence of normal bone-remodeling activity (3). The elevated osteoclast function is also associated with many other disorders of the skeleton, including periodontal disease, rheumatoid arthritis, and the metastatic spread of cancer to bone (4).

Studies in animal models of osteopetrosis, and particularly in mutant mice, have provided significant new insights regarding the fundamental biology of osteoclasts (1, 5, 6). For example, some mutants completely lack osteoclasts, implying the involvement of the mutated genes in the early stages of osteoclast differentiation (7–10); other mutants produce osteoclasts with an immature appearance, highlighting the important roles of these mutated genes in terminal differentiation (11, 12); other mutants produce osteoclasts that appear normal but are defective in their ability to resorb bone, indicating that these genes are required for the maturation of the osteoclast and their normal bone-resorption capacity (13–17). These three different types of osteopetrosis mutants are phenotypically quite similar, except that the first appears to have reduced bone formation, suggesting that the absence of osteoclasts may also affect the activity of osteoblasts in these mice (18). This group of mutants is phenotypically reminiscent of human autosomal-recessive osteopetrosis. The mouse genes *Atp6i*, *Gl*, *Traf-6*, *c-Src*, and *Clcn-7*, respectively, when mutated, give rise to osteopetrosis with abnormal osteoclasts (13–17, 19). The human homologues for three of these genes (*GL*, *ATP6i*, and *CLCN-7*, respectively) are in fact disease genes for human autosomal-recessive osteopetrosis (13, 14, 19). However, mutations in these three genes alone do not appear to account for all cases of this disease in humans (13, 14, 19), indicating the existence of additional disease-causing genes for autosomal-recessive osteopetrosis.

Osteoclasts are also vital for tooth eruption, a process that requires two highly coordinated processes: the formation of an eruption pathway; and the vertical movement of the developing tooth bud into the oral cavity (20). To form the eruption pathway, active alveolar bone resorption and the recruitment of numerous osteoclasts are required (21). Furthermore, recent studies have shown that a number of genes contribute to this process (21). Interestingly, we know very little about tooth root formation, an important physiological process. There are numerous osteopetrosis models but it is, in fact, not known whether or not these animals have defects in tooth root formation, and whether osteoclasts play any role in this developmental event.

In this work, we have characterized a new mouse model of osteopetrosis that is caused by a spontaneous mutation: it is referred to as *ntl* (‘new toothless’) mouse. First, we investigated

whether, how, and why odontomas were developed in this mutant. Second, we attempted to identify, by genetic mapping, the gene that is responsible for this osteopetrosis animal model. Third, we considered whether this model and other similar osteopetrosis models interfere with tooth root formation. Our results support the hypotheses that defects in osteoclasts disrupt the development and growth of the tooth root, and that homeostatic perturbation of the odontogenic precursors that are central to the root formation of mouse incisors is the primary cause of odontoma-like proliferations in this new mutant.

Material and methods

Mice were housed in our specific pathogen-free (SPF) facility. After weaning, the *ntl* mutant mice were fed with the liquid diet Peptamin (Nestle Nutrition, Minnetonka, MN, USA). All procedures involved in the animal experiments were approved by the Institutional Animal Care and Use Committee at Case Western Reserve University.

Linkage analysis

The chromosomal location of the mutant allele was determined using standard genetic mapping experiments. Briefly, we took advantage of the fact that the mutant phenotype is fully penetrant not only in a *C57 BL/6j-129 Sv* mixed background but also in either the *C57 BL/6j* or the *129 Sv* inbred background, and that an extensive number of *Mit* alleles, which are polymorphic between these two inbred strains, are available. Specifically, we first introduced the mutant allele into either the *C57 BL/6j* or the *129 Sv* inbred strains by backcrossing so that the mutant allele was placed among a set of *Mit* markers that are distinguishable between the *C57 BL/6j* and the *129 Sv* strains. Individuals carrying the mutant allele were identified based on their ability to produce homozygous mutants when mated with a mutant allele carrier. These mice were intercrossed to generate homozygous mutant mice. Genotyping analyses were then used to determine which markers co-segregated with the mutant allele, that is, these markers were present at a higher frequency among the homozygous mutants when compared with both the wild-type (WT) and heterozygous littermates. These *Mit* markers were then identified as being located in the same chromosomal region as this mutant allele. The likelihood of this co-segregation between a given marker and this mutant phenotype reflects the genetic distance between this known *Mit* marker and the mutant allele. However, because heterozygous carriers could only be identified by progeny testing, only homozygous mutants were used in our linkage analysis. Thus, for each given experiment, the number of informative gametes is equal to the number of homozygous mutant mice obtained. The genetic distance between a known *Mit* allele and the mutant allele is calculated as the percentage of mutant mice for which the *Mit* allele did not co-segregate.

Selection of *Mit* alleles and polymerase chain reaction genotyping

For the genetic linkage analysis experiments, *Mit* alleles that are polymorphic between the *129 Sv* and the *C57 BL/6j* inbred strains were first selected if the *129 Sv* and the *C57 BL/6j* alleles could be readily distinguished by a simple electrophoretic analysis in a 4% Tris/Borate/EDTA (TBE) agarose gel. Specifically, polymerase chain reaction (PCR) products were electrophoresed through a 4% agarose gel in 1 × TBE buffer containing ethidium

bromide at 8 volts cm^{-1} for 15 min. After electrophoresis, the PCR products were visualized under ultraviolet (UV) light to determine the genotype of individual samples. All oligonucleotide primers, except for *D17Mit133*, were synthesized based on the information obtained from the UniSTS database (http://www.ncbi.nlm.nih.gov/sites/entrez?db=unists). Because the primer set for marker D17Mit313 cannot distinguish between C57BL/6j and 129 Sv, we modified the reverse primer to 5′-CCT CAC ACA GCC AAT GCA GAA TCT-3′.

Embryonic liver transplantations

Five-day-old pups from a cross between mice that were heterozygous for both the *ntl* mutant allele and the *Mit133* allele were irradiated with 400 cGy administered from a ^{137}Cs source. Four hours later the mice were transplanted with 1×10^6 or 5×10^6 embryonic liver cells derived from 16.5 days postcoitum (dpc) embryos of the same genetic background. The cells were suspended in 30 μl of phosphate- buffered saline and injected intraperitoneally into the mice. The mice were killed 5 wk after transplantation of the liver cells and examined radiographically and histologically. The homozygous *ntl* mutants were identified using PCR-based genotyping for the *129-Mit133* allele, which is tightly linked to the *ntl* mutant allele.

In vitro culture of osteoclasts

Osteoclasts were generated by the co-culture of splenocytes from 4-wk-old mice with either ST2 cells and $1.25(OH)_2$ vitamin D_3 or in the presence of recombinant macrophage colony-stimulating factor (M-CSF) and receptor activator of nuclear factor-κB ligand (RANKL) supplements, as described previously (22). Specifically, the ST2 co-culture method was used in the *in vitro* bone-resorption experiments as well as in those for monitoring the differentiation of osteoclasts, while the M-CSF/RANKL supplement method was used to obtain highly enriched osteoclast preparations for RNA or protein extraction, unless specified otherwise. In the experiments using the co-culture method, individual pairs of a mutant and a control were used to initiate two separate *in vitro* cultures in 48-well plates and to compare the differentiation of osteoclasts and bone resorption between the cells derived from these two different sources. The experiment was repeated four times. The M-CSF/RANKL supplement method was used to induce osteoclast formation either with tissue culture slides containing 2-cm^2 chambers for easy microscopic observations or in 10-cm culture dishes for RNA or protein extraction. In the former, 1×10^5 splenic cells were placed in each 2-cm^2 chamber, whereas in the latter, splenic cells from five mutant mice and five WT mice, respectively, were pooled and cultured on 10-cm culture dishes. All cultures were initiated in medium containing Dulbecco's modified Eagle's minimal essential medium (DMEM) supplemented with 10% fetal calf serum (FCS), 20 ng ml^{-1} of human M-CSF (R&D Biosystems, Minneapolis, MN, USA), 50 ng ml^{-1} of RANKL + 50 μg ml^{-1} of ascorbate + 100 nM dexamethasone. Three days later, the old medium was replaced with fresh inducing medium containing MEM supplemented with 50 ng ml^{-1} of M-CSF + 50 ng ml^{-1} of RANKL + 50 μg ml^{-1} of ascorbate + 100 nM dexamethasone. The cultures were processed for analysis on day 6. Also in the latter case, for each genotype, one plate was used to perform tartrate-resistant acid phosphate (TRAP) staining to estimate the

contribution of TRAP-positive osteoclasts. With our protocol, TRAP-positive cells accounted for approximately 95% of the total populations in both the WT and the mutant.

In vitro bone-resorption assay

The experimental procedure for the *in vitro* bone-resorption assay was very similar to that for the *in vitro* culture of the osteoclast experiments described above, except that one ivory slice was added to each culture in the *in vitro* bone-resorption assay (22). Ivory slices were prepared from trimmed elephant tusks provided by the Cleveland MetroPark Zoo. After 9 d of co-culture, a set of slices was processed for TRAP staining. Another set of slices was incubated with the cells for another 3 d and then stained with Toluidine Blue. The ivory slices were then examined under a Leica FLUOTM GFP microscope (Diagnostic Instruments, Sterling Heights, MI, USA) and pictures of the slices were taken using an RT COLOR SPOT digital camera (Diagnostic Instruments) attached to the microscope. The experiment was repeated four times.

Immunohistochemistry

Immunostaining of amelogenin (polyclonal antibodies against amelogenin were kindly provided by Dr Jan Hu of the University of Michigan, Ann Arbor, MI, USA) (23) and of dentin sialophosphoprotein (DSPP) (polyclonal antibodies against DSPP were kindly provided by Dr Chunlin Qin at Baylor College of Dentistry, Dallas, TX, USA) (24) were performed on paraffin sections. Immunological reactions were visualized using a Vector ABC kit (Vector, Burlingame, CA, USA) and a peroxidase diaminobenzidine reaction. The tissue slices were mounted on glass slides and hematoxylin counterstaining was used (25).

Scanning electron microscopy

Bone tissues were fixed in 70% ethanol and embedded in methyl-methacrylate (MMA; Buehler, Lake Bluff, IL, USA). The surface of the MMA-embedded bone was polished, coated with gold and palladium, and examined using an FEI/Philips XL30 Field emission environmental scanning electron microscope (FEI/Philips, Hillsboro, OR, USA), as previously described (26).

Goldner trichrome stain and Toluidine Blue stain

Femurs from both WT mice and mutant mice were removed and fixed in 10% formalin for 48 h at room temperature. The specimens were dehydrated through a graded series of ethanol (70–100%) and embedded in MMA without prior decalcification. Undecalcified thin (6 μm) long-bone sections were cut and adhered to charged glass slides. After deplasticizing, the sections were stained with either Toluidine Blue (see the protocol online: http://depts.washington.edu/rubelab/protocols/Toluidine-Blue.html) or Goldner's trichrome stain (see the protocol online: http://www.emsdiasum.com/microscopy/technical/datasheet/26386.aspx) for identification of the mineralized and nonmineralized bone as well as evaluation of osteoclast morphologies.

TRAP staining

Tartrate-resistant acid phosphate staining was performed using a TRAP staining kit (Sigma, St Louis, MO, USA). Tartrate-resistant acid phosphate activity was detected according to the procedure with naphthol AS-TR phosphate containing 10 mML(+)-tartaric acid as the substrate. In the case of TRAP staining on paraffin-embedded bone sections, the slides were counterstained with methyl green after the completion of TRAP staining. The specimens were then viewed under a Nikon E800 microscope (Nikon, Melville, NY, USA) and photographed using a micropublisher 3.3 camera (Qimaging, Burnaby, BC, Canada).

Analyses of *Clcn7* gene expression

For mutation screening experiments, complementary DNA (cDNA) of mouse *Clcn7* was amplified using reverse transcription–polymerase chain reaction (RT-PCR) as four overlapping fragments and then sequenced using the following primers (note: the number in the name of each primer represents the 5′-end position in the mouse *Clcn 7* messenger RNA (mRNA) (accession number: NM_011930): 1) Mc1t-35: 5′-gctgccggtctgccggctgtt-3′; 2) Mc1b-805: 5′-gccagtccccctaccacagac-3′; 3) Mc2t-742: 5′-gcggctcaagacgctggt- 3′; 4) Mc2b-1575: 5′-cagcaggccaggaagaagtaga-3′; 5) Mc3t-1481: 5′-cacccctgagaagagcgttgt-3′; 6) Mc3b-2286: 5′-ggtccatggtgcattcacgct-3′; 7) Mc4t-2233: 5′-cccaatccagtccattc atgt-3′; 8) Mc4b-2530: 5′-ggctggggtactgcatgtcca-3′. Total RNA samples extracted from both the kidneys of 4-wk-old mice and from *in vitro*-differentiated, TRAP-positive cells were used as templates. Each of these experiments was performed twice with two different sets of mice. Thus, a total of four sets of animals were examined. For every RT-PCR reaction, the target product was purified and sequenced (both strands were sequenced). To study Clcn7 protein expression, proteins were extracted from different tissues/organs of 4-wk-old mice or from *in vitro*-cultured splenic cells that were enriched in TRAP-positive cells (see the section above for detail). Three different antisera, *C15-sc16444*, *N-20-sc16442* (Santa Cruz Biotechnology, Santa Cruz, CA, USA), and rabbit antiserum *N-11753* (14), were used in the western blot experiments. The *N-11753* antibody was kindly provided by Dr T. J. Jentsch. Anti-(gamma tubulin) IgG (Santa Cruz) were used in the control experiments to verify the relative amount of total proteins loaded for each sample. Each of these experiments was also repeated at least once with a different set of mice.

Radiography and histological preparation

Wild-type and homozygous mutant mice were examined on a Faxitron model MX-20 Specimen Radiography System with a digital camera attached (Faxitron X-Ray, Lincolnshire, IL, USA). Femur specimens from WT mice and homozygous mutant mice were dissected and fixed in 4% paraformaldehyde at 4°C overnight, then treated using two different processes: (i) one femur was demineralized in 10% EDTA solution (Sigma) over 2 wk, then dehydrated, embedded in paraffin, and sectioned at a thickness of 6 μm; and (ii) the other femur was dehydrated with a series of graded ethanol and embedded in methyl methacrylate with 15% dibutyl phthalate (Fisher Scientific, Pittsburgh, PA, USA). Undecalcified sections (8 μm) were cut using a Supercut 2050 microtome (Reichert-Jung, Heidelberg, Germany) and adhered to charged glass slides before staining with Goldner’s

trichrome stain for evaluation of osteoclasts and their lacunae; the adhered sections were also stained with Toluidine Blue to identify ruffled borders of osteoclasts.

Results

The discovery of a new spontaneous autosomalrecessive osteopetrosis mouse strain

In our regular maintenance of a Bloom syndrome (*Blm)* knockout mouse line (27), runted progeny were identified among healthy siblings. This runted phenotype was never observed among *Blm* knockout mice and was not segregated with the *Blm* knockout allele (data not shown). These runted mice died shortly after weaning. All lacked erupted teeth (Fig. 1A, right), suggesting that these mice might represent a new osteopetrosis mutant. Hepatosplenomegaly was observed in all animals examined, but the degree of severity varied among individuals. Analysis of 96 progeny from 14 litters resulted in the identification of 25 progeny with the osteopetrotic phenotype (26%), indicating that this phenotype is an autosomal-recessive trait. Judging by the above features, these mutant mice appeared to represent a new model for autosomal-recessive osteopetrosis. We designated this new mutant as the ‘new toothless’, or *ntl*, mouse.

Interestingly, when fed a liquid diet, the mutant mice were able to survive to adulthood (up to 18 months) and were actually fertile despite severe osteopetrosis phenotypes. Indeed, like other osteopetrosis mouse models, these mice have little bone marrow cavity and thin cortical bone, based on the following evidence. X-ray radiography analysis of these mice revealed a generalized high bone density throughout the entire skeletal system with a club-shaped characteristic (Fig. 1B, right panel), a hallmark of infantile malignant autosomal-recessive osteopetrosis (ARO; MIM 259700). Scanning electron microscopy images showed that the mutant femur consisted primarily of primitive trabecular bone without a prominent bone marrow space (Fig. 1C, right panel) with a cortical bone that was much thinner than that of the WT control (Fig. 1D, lower panel). The lack of prominent bone marrow space in the mutant was particularly evident by the opaque appearance of their long bones (Fig. 1C).

Genetic mapping of the mutation to a 3.2 cM interval on mouse chromosome 17

Having determined that the *ntl* mouse is a model of autosomal-recessive osteopetrosis, we then investigated whether the mutant arose as a result of a mutation in a novel osteopetrosis gene or as a unique mutation in one of the five known osteopetrosis genes. First, we investigated whether the mutant allele represents a mutated version of any of the known osteopetrosis genes (i.e. *Gl*, *c-src*, *Traf-6*, *Clcn-7*, and *Atp6i*). Specifically, we examined whether the mutation would co-segregate with any of these genes by conventional genetic linkage analysis experiments. The mutant was originally identified in a 129Sv × C57 BL/6j mixed genetic background. Thus, in order to conduct linkage-analysis experiments, the mutant allele had to be introduced into the C57 BL/6j or 129 Sv inbred genetic background, respectively. Importantly, after the allele was introduced into the C57 BL/6j or 129 Sv inbred background, osteopetrosis mutant mice that were undistinguishable from those in the original 129Sv × C57 BL/6j mixed genetic background could still be obtained. Moreover, the mutant phenotype remained fully penetrant (data not shown). Thus, intercrosses between 129 inbred mice and mice carrying the mutant allele in the C57 BL/6j inbred background

produced individuals desirable for genetic linkage experiments, as they are informative with respect to all alleles that are polymorphic between the 129 Sv and C57 BL/6j inbred strains. The result of an initial study excluded *Gl*, *c-src*, *Traf-6*, and *Atp6i* as potential candidates for the disease-causing gene, but revealed a strong linkage to the *Clcn-7* locus (Table 1). A further genetic mapping analysis with a larger cohort of animals confirmed the linkage between the new mutant allele and the *Clcn7* locus (Fig. 2A). Specifically, 1, 0, and 2 crossovers between the mutant allele and the *D17Mit213*, *D17Mit133*, and *D17Mit80* alleles were detected by analyzing 96, 91, and 92 informative gametes, respectively. These data placed the mutant allele within a 3.2 cM genetic interval between *D17Mit213* and *D17Mit80* on mouse chromosome 17, a region that also contains the *Clcn-7* gene (Fig. 2A).

The region between *D17Mit213* and *D17Mit80* encompasses approximately 10 mega base pairs of mouse chromosome 17. Moreover, the proximal portion of this region appears to be refractory to crossover, hindering the effort to further narrow down the candidate region. Conversely, because loss-of-function mutations in *Clcn-7* have previously been associated with osteopetrosis (14), the detection of a tight linkage between the mutant allele and the *Clcn-7* locus suggests that *Clcn-7* could be the disease-causing gene in the mutant mice. To address this possibility, we first sequenced the *Clcn-7* cDNA and the corresponding genomic DNA from the mutant. The results showed that there were no mutations within the *Clcn-7* cDNA, excluding the possibility that the mutant is caused by a mutation within the coding sequence of *Clcn-7* that might have compromised the function of Clcn-7. However, it remains possible that the mutant may stem from a mutation in the non-coding region, which altered the level of expression of the *Clcn-7* gene. In this case, a change in the level of Clcn-7 protein would be expressed. However, western blot analyses of samples from a number of sources of both WT mice and the mutant mice, including *in vitro*-cultured osteoclasts as well as several *in vivo* organs and tissues, did not detect any significant differences in Ccln-7 expression between the WT and the mutant (Fig. 2B,C and data not shown), ruling out the possibility that the mutant phenotype is caused by a significant change in the steady-state level of Clcn7 protein expression. Therefore, together these data indicate that the mutant is not caused by a conventional mutation in the *Ccln-7* gene, the only known osteopetrosis gene within the *Ntl* candidate region. This conclusion is consistent with the distinctive phenotypes between the *ntl* mutants and *Clcn-7* knockout mice. For example, *Clcn-7* knockout mice died shortly after birth because of a defect in the central nervous system (CNS) (28), while *ntl* mice could survive to adulthood and were fertile. Thus, the *ntl* mutant represents a novel osteopetrosis mouse model.

Absence of tooth roots and development of odontoma in the mutant mice

While searching for the *Ntl* candidate gene, we noticed that aged *ntl* mice developed an unusual growth pattern around the face at approximately 4 months of age. This observation, plus the indication that the *ntl* mice might represent a novel osteopetrosis mouse model, prompted us to investigate this new mutant further.

Radiographic images of the 5-wk-old mutant lower jaw showed neither tooth eruption nor tooth root formation (Fig. 3A, lower level). Histology of the first mutant molar further confirmed a lack of tooth roots in the mutant (Fig. 3B, right panel). Because odontoma-like

proliferations are a common feature of osteopetrosis (20), we next examined whether the unusual growth in the facial area of the *ntl* mice was caused by the development of odontoma-like proliferations. The animals were fed a liquid diet and were killed at the age of 7 months. Representative photographs (Fig. 3C) show the presence of extensive odontoma-like proliferations around the malformed roots of the incisors, in both the mandible and maxilla of the mutant mice.

By definition, odontoma-like proliferations should contain both enamel and dentin components. To test this, we stained these tissues using an antibody against amelogenin, a marker for enamel (Fig. 4A, right panel, arrows), and an antibody against DSPP, a marker for dentin (Fig. 4A, left panel, arrows). We found that amelogenin (Fig. 4B) and DSPP (Fig. 4C) are highly expressed in the odontoma-like proliferations.

By contrast, no molar-associated odontoma-like proliferations were found in these mice, regardless of their age.

We also investigated whether the development of odontoma-like proliferations in the *ntl* mice were related to abnormal tooth development, because abnormal tooth development, particularly abnormal tooth root formation, is a common feature of osteopetrotic mutant mice and has been implicated in the etiology of odontoma in humans (29). As shown in Fig. 3A,B all mutant mice displayed a lack of tooth root formation.

The osteopetrosis phenotype is caused by an intrinsic defect in osteoclast-mediated bone resorption

An osteopetrosis phenotype may be caused by an intrinsic defect in the osteoclasts or by an extrinsic defect in the stromal cell compartment (8). Tartrate-resistant acid phosphate staining experiments revealed that TRAP-positive cells were detected on sections of bones from both the mutant mice and WT mice (Fig. 5A). In both cases, osteoclasts had multiple nuclei (Fig. 5A–C), indicating that they represented differentiated osteoclasts. However, the mutant osteoclasts lacked well-defined resorption lacunae, which were observed beneath the osteoclasts from WT mice (Fig. 5B). Furthermore, prominent osteoclast-associated ruffled borders were detected in WT mice, but not in the mutant mice (Fig. 5C, right panel). These observations suggest that the resorption defect was not caused by the absence of osteoclasts. Instead, it is probably caused by a defect in osteoclast-mediated bone resorption.

To determine the resorption capacity of mutant osteoclasts, we cultured spleen cells from the mutant mice and WT littermates on bone slices *in vitro*. Mutant spleen cells, when cultured in the presence of M-CSF/RANKL, formed a similar number of TRAP-positive osteoclasts as formed by WT cells (Fig. 6A). However, unlike their WT counterparts, these cells failed to form resorption pits when co-cultured with ST-2 stromal cells on ivory sections (Fig. 6B). Quantitative data confirmed no apparent difference in osteoclast numbers between the WT and mutant cells, but osteoclasts derived from mutant cells formed no resorption pits (Fig. 6C). Thus, the mutant osteoclast precursors had the ability to differentiate into almost mature osteoclasts, but they were defective in bone resorption.

Transplantation of live fetal cells rescues the mutant mice

To confirm that the above defects are indeed osteoclast autonomous, we performed osteoclast precursor transplantation experiments in neonate (5-d-old) mutant mice using osteoclast progenitor cells isolated from WT fetal liver. Radiograph imaging analysis of these mice at 5 wk of age demonstrated that the various osteopetrosis features in the untreated mutant mice (Fig. 7A, middle panel) were rescued (Fig. 7A, right panel). Notably, the teeth were erupted and their roots had formed (Fig. 7B, lower panel). Histological data not only further confirmed this observation, but also showed that the osteoclast number in the mutant mouse injected with the WT osteoclast progenitors (Fig. 7C, TRAP staining, lower panel) returned to a level comparable with that in the WT control (Fig. 7C, upper level). Furthermore, the central spongiosa (bone marrow spaces for the tooth root) was restored in both molars and the incisor in the rescued mandible, as demonstrated by X-ray and histological images (Fig. 7B,C), supporting an intrinsic defect in osteoclast-mediated bone resorption. Yet, the proximal regions of the mutant incisors end before the first molar (M1), whereas those of the WT extend to underneath the third molar (M3).

Discussion

We have reported the identification of a spontaneous mouse mutant, the *ntl* mouse, which has severe autosomal- recessive osteopetrosis. Phenotypic characterization revealed that this mutant displays all the features that are characteristic of osteopetrosis, including absence of bone resorption, lack of tooth eruption, bone marrow filled with trabecular bone, and focal fusion of incisors to the adjacent bone leading to odontoma-like proliferations, comparable to odontoma in humans. Importantly, our results from genetic and molecular biology studies strongly suggest that this new mutant represents a novel model for type II autosomal-recessive osteopetrosis. Furthermore, the long-lived nature of these *ntl* osteopetrosis mice, when maintained on a soft diet, enabled us to establish an unambiguous link between abnormal tooth development and the susceptibility to odontoma-like proliferations in mice.

Osteoclasts are essential for tooth eruption (30). Interestingly, the osteopetrotic phenotype, but not the defect in tooth eruption, is spontaneously restored in *op/op* mice with age (31, 32). Yoshino and colleagues (33) reported that neutralizing antibody against M-CSF inhibited incisor eruption in C57B6 inbred mice, as long as it was administered before embryonic day 16.5. If the same antibody was given to mice 1 d later, its inhibitory effect on incisor eruption was lost, even though it still inhibited osteoclast formation. Based on this finding, they hypothesized that there may be a critical period (between embryonic days 15.5 and 16.5), during which the presence of osteoclasts is essential for incisor eruption. However, we have shown in the present study that intraperitoneal injections of WT osteoclast progenitor cells after birth (after the ‘critical period’) rescued the osteopetrosis, as well as the defect of tooth eruption, in both incisors and molars in these mutant mice (Fig. 7), arguing against this simple model and indicating that obstructed tooth buds, at least those in the *ntl* mice, remain competent for eruption after birth. This rescue is also consistent with the fact that in rodents, the eruption of the first molar occurs at approximately 2 weeks after birth.

In contrast to the roles of osteoclast-mediated bone resorption in tooth eruption, the significance of osteoclasts in tooth root formation is less well defined. Yet, it is widely believed that an extension of the inner and outer dental epithelia in the tooth cervical loop, namely the Hertwig's epithelial root sheath, probably initiates differentiation of odontoblasts from the peripheral mesenchymal cells followed by tooth root formation. Interestingly, there is no report of successful attempts to induce tooth root formation either *in vitro* or *in vivo*, although significant progress has been achieved in regenerating the tooth crown (34). In the present study, we demonstrated that osteoclasts play an essential role in root formation. First, the mutant mice with abnormal osteoclasts displayed no tooth roots (Figs 3,7). Second, intraperitoneal injections of osteoclast progenitors into the mutant mice restored both osteoclast function and the tooth roots in both incisor and molars (Fig. 7). Third, the central spongiosa region surrounding the tooth root was reformed after intraperitoneal injections of the WT osteoclast precursors (Fig. 7). Fourth, lack of tooth root formation was observed in three additional osteopetrosis models, namely RANK knockout mice, RANKL knockout mice (Fig. S1), and *c-src* knockout mice (35).

The partial rescue of incisor roots is probably a result of the timing factor. During normal development, the proximal end of the mouse incisor has already extended underneath the first molar at day 5 postnatally, and will continue to grow inside the jaw until it reaches the level of the third molar. Because the molar root formation starts a few days later, it is very likely that transplantation of embryonic liver cells at a later stage (e.g. P15 or P20) may not be able to rescue the molar root as efficiently as early stage transplantation (P5).

Based on the above observations, we propose a model to explain the importance of osteoclasts in the tooth root formation process (Fig. 8): tooth root formation comprises at least two phases: (i) formation of sufficient space in the central spongiosa where future tooth roots will be held in the jaw, which requires osteoclast bone resorption; and (ii) formation of the tooth root, which may or may not require osteoclasts. Clarifying whether osteoclasts (or bone marrow cells) directly interact with tooth progenitor cells will be our next goal in future studies.

Another frequent feature of osteopetrosis is development of odontoma-like proliferations around the base of the unerupted incisors (35–37). This was explained as a result of the invasion of alveolar bone trabeculae into the tooth germs (36). Interestingly, we did not observe any odontoma-like proliferations around the molars in the mutant mice, even when they were 18 months of age (data not shown). This difference in the propensity of developing odontoma-like proliferation around unerupted incisors, but not at the unerupted molars, in mice, is probably because the odontogenic epithelium in molars has limited growth capacity, whereas the incisor grows continuously throughout the life span of the rodents. In other words, molars do not erupt continuously, and thus the machinery to cause these lesions is missing. Thus, we propose that the perturbation of the homeostasis of the tooth root odontogenic precursors, rather than that of the tooth germs, is primarily responsible for the development of odontoma-like proliferations. More specifically, we propose that in osteopetrotic mice, the pronged residency of the odontogenic cells in an unnatural microenvironment within the primitive trabeculae matrix, rather than in the usual central spongiosa surrounding, causes the abnormal proliferation of these precursors and the

eventual development of odontoma-like overproliferation (Fig. 8B). It should be noted, however, that the association of odontomas with abnormal primary tooth eruption has also been documented in humans, although it only accounts for approximately 1.25% of compound odontomas (29), suggesting that the etiology of odontomas may be different between humans and the *ntl* mice.

The genetic mapping data place the novel osteopetrosis mutant allele within a genetic interval of 3.2 cM, which also contains the *Clcn7* gene, the only known osteopetrosis gene within this region. We show here that this mouse mutant lacks a *de novo* mutation within the coding region of its *Clcn7* gene and has a Clcn7 protein expression level in its osteoclasts that is similar to that of its WT counterpart. More importantly, *ntl* mutant mice and *Clcn-7* knockout mice are clearly phenotypically distinct. These data argue against the possibility that the mutant carries a conventional *Clcn7* mutation, and strongly suggest the involvement of a previously unknown osteopetrosis disease-causing allele, although it remains possible that the mutant could be the result of an unconventional type of mutation that severely compromises the normal function of the *Clcn-7* gene. Interestingly, an osteopetrosis locus, the osteopetrotic locus of a spontaneous rat mutant, has been localized to a region that is tightly linked to, but does not include, the rat *Clcn-7* gene (38), indicating the presence of yet another osteopetrosis gene near *Clcn-7*. The synteny regions around the *Clcn-7* genes of rat and mice are highly conserved. Thus, it is possible that a novel osteopetrosis gene that is tightly linked to *Clcn-7* also exists in mice.

Localization of the mutation to a genetic interval of < 3.2 cM, and the indication of the involvement of a novel disease-causing allele in this spontaneous mutant, shall justify the next step to clone this novel osteopetrosis disease-causing mutation. A survey of the annotated genes within this region revealed a number of potential candidate genes, including *Atp6v0c*, *Cacna1h*, and *Rab26*. *Atp6v0c* encodes a subunit of the V-H-ATPase complex. Mutations in the gene coding for the ATP6i subunit of this complex caused osteopetrosis, both in mice and in humans (39). *Cacna1h* encodes a T-type Ca^{2+} channel. A recent study showed that the epithelial Ca^{2+} channel, TRPV5, is essential for proper osteoclast bone resorption (40). Rab26 is a member of the Rab subfamily of small GTP-binding proteins. Members of this subfamily play important roles in osteoclast- mediated bone resorption (41). However, a preliminary analysis, using semiquantitative RT-PCR, on the expression of these genes failed to detect any major difference between WT and mutant osteoclasts. In addition, sequencing analysis on the coding regions of these three genes did not identify any mutations that were co-segregated with the mutant phenotype. These preliminary results do not indicate any of these genes as a strong candidate responsible for the osteopetrosis disease- causing mutation. Thus, further fine-mapping experiments will be necessary to define the candidate interval to a smaller region before applying a candidate gene approach.

Supplementary Material

Refer to Web version on PubMed Central for supplementary material.

Acknowledgments

The authors wish to thank Drs Joseph Nadeau and Matthew L. Warman for advice and support during this study; and the Cleveland Metropark Zoo for supplying the ivory used in this study. Support for this research was provided by the Searle Scholar Program (to G.L.), and grants AR51587 and DE015209 (to J.Q.F) from the National Institutes of Health.

References

1. Karsenty G, Wagner EF. Reaching a genetic and molecular understanding of skeletal development. Dev Cell. 2002; 2:389–406. [PubMed: 11970890]
2. Lazner F, Gowen M, Pavasovic D, Kola I. Osteopetrosis and osteoporosis: two sides of the same coin. Hum Mol Genet. 1999; 8:1839–1846. [PubMed: 10469835]
3. de Vernejoul MC, Benichou O. Human osteopetrosis and other sclerosing disorders: recent genetic developments. Calcif Tissue Int. 2001; 69:1–6. [PubMed: 11685426]
4. Boyle WJ, Simonet WS, Lacey DL. Osteoclast differentiation and activation. Nature. 2003; 423:337–342. [PubMed: 12748652]
5. Marks SC Jr. Osteoclast biology: lessons from mammalian mutations. Am J Med Genet. 1989; 34:43–54. [PubMed: 2683780]
6. McLean W, Olsen BR. Mouse models of abnormal skeletal development and homeostasis. Trends Genet. 2001; 17:S38–S43. [PubMed: 11585675]
7. Johnson RS, Spiegelman BM, Papaioannou V. Pleiotropic effects of a null mutation in the c-fos proto-oncogene. Cell. 1992; 71:577–586. [PubMed: 1423615]
8. Kong YY, Yoshida H, Sarosi I, Tan HL, Timms E, Capparelli C, Morony S, Oliveira-dos-Santos AJ, Van G, Itie A, Khoo W, Wakeham A, Dunstan CR, Lacey DL, Mak TW, Boyle WJ, Penninger JM. OPGL is a key regulator of osteoclastogenesis, lymphocyte development and lymph-node organogenesis. Nature. 1999; 397:315–323. [PubMed: 9950424]
9. Tondravi MM, McKercher SR, Anderson K, Erdmann JM, Quiroz M, Maki R, Teitelbaum SL. Osteopetrosis in mice lacking haematopoietic transcription factor PU. 1. Nature. 1997; 386:81–84. [PubMed: 9052784]
10. Yoshida H, Hayashi S, Kunisada T, Ogawa M, Nishikawa S, Okamura H, Sudo T, Shultz LD, Nishikawa S. The murine mutation osteopetrosis is in the coding region of the macrophage colony stimulating factor gene. Nature. 1990; 345:442–444. [PubMed: 2188141]
11. Hodgkinson CA, Moore KJ, Nakayama A, Steingrimsson E, Copeland NG, Jenkins NA, Arnheiter H. Mutations at the mouse microphthalmia locus are associated with defects in a gene encoding a novel basic-helix-loop-helix-zipper protein. Cell. 1993; 74:395–404. [PubMed: 8343963]
12. Thesingh CW, Scherft JP. Fusion disability of embryonic osteoclast precursor cells and macrophages in the microphthalmic osteopetrotic mouse. Bone. 1985; 6:43–52. [PubMed: 3994857]
13. Chalhoub N, Benachenhou N, Rajapurohitam V, Pata M, Ferron M, Frattini A, Villa A, Vacher J. Grey-lethal mutation induces severe malignant autosomal recessive osteopetrosis in mouse and human. Nat Med. 2003; 9:399–406. [PubMed: 12627228]
14. Kornak U, Schulz A, Friedrich W, Uhlhaas S, Kremens B, Voit T, Hasan C, Bode U, Jentsch TJ, Kubisch C. Mutations in the a3 subunit of the vacuolar H(+)-ATPase cause infantile malignant osteopetrosis. Hum Mol Genet. 2000; 9:2059–2063. [PubMed: 10942435]
15. Li YP, Chen W, Liang Y, Li E, Stashenko P. Atp6i-deficient mice exhibit severe osteopetrosis due to loss of osteoclast-mediated extracellular acidification. Nat Genet. 1999; 23:447–451. [PubMed: 10581033]
16. Lomaga MA, Yeh WC, Sarosi I, Duncan GS, Furlonger C, Ho A, Morony S, Capparelli C, Van G, Kaufman S, van der Heiden A, Itie A, Wakeham A, Khoo W, Sasaki T, Cao Z, Penninger JM, Paige CJ, Lacey DL, Dunstan CR, Boyle WJ, Goeddel DV, Mak TW. TRAF6 deficiency results in osteopetrosis and defective interleukin-1, CD40, and LPS signaling. Genes Dev. 1999; 13:1015–1024. [PubMed: 10215628]

17. Soriano P, Montgomery C, Geske R, Bradley A. Targeted disruption of the c-src proto-oncogene leads to osteopetrosis in mice. Cell. 1991; 64:693–702. [PubMed: 1997203]
18. Karsdal MA, Martin TJ, Bollerslev J, Christiansen C, Henriksen K. Are nonresorbing osteoclasts sources of bone anabolic activity? J Bone Miner Res. 2007; 22:487–494. [PubMed: 17227224]
19. Sobacchi C, Frattini A, Orchard P, Porras O, Tezcan I, Andolina M, Babul-Hirji R, Baric I, Canham N, Chitayat D, Dupuis-Girod S, Ellis I, Etzioni A, Fasth A, Fisher A, Gerritsen B, Gulino V, Horwitz E, Klamroth V, Lanino E, Mirolo M, Musio A, Matthijs G, Nonomaya S, Notarangelo LD, Ochs HD, Superti Furga A, Valiaho J, van Hove JL, Vihinen M, Vujic D, Vezzoni P, Villa A. The mutational spectrum of human malignant autosomal recessive osteopetrosis. Hum Mol Genet. 2001; 10:1767–1773. [PubMed: 11532986]
20. Ten Cate, A. Oral histology: development, Structure, and Function. St. Louis: Mosby; 1998.
21. Wise GE, Frazier-Bowers S, D'Souza RN. Cellular, molecular, and genetic determinants of tooth eruption. Crit Rev Oral Biol Med. 2002; 13:323–334. [PubMed: 12191959]
22. Ragab AA, Lavish SA, Banks MA, Goldberg VM, Greenfield EM. Osteoclast differentiation requires ascorbic acid. J Bone Miner Res. 1998; 13:970–977. [PubMed: 9626628]
23. Simmer JP, Lau EC, Hu CC, Aoba T, Lacey M, Nelson D, Zeichner-David M, Snead ML, Slavkin HC, Fincham AG. Isolation and characterization of a mouse amelogenin expressed in Escherichia coli. Calcif Tissue Int. 1994; 54:312–319. [PubMed: 8062146]
24. Qin C, Brunn JC, Cadena E, Ridall A, Tsujigiwa H, Nagatsuka H, Nagai N, Butler WT. The expression of dentin sialophosphoprotein gene in bone. J Dent Res. 2002; 81:392–394. [PubMed: 12097430]
25. Lu Y, Ye L, Yu S, Zhang S, Xie Y, McKee MD, Li YC, Kong J, Eick JD, Dallas SL, Feng JQ. Rescue of odontogenesis in Dmp1-deficient mice by targeted re-expression of DMP1 reveals roles for DMP1 in early odontogenesis and dentin apposition *in vivo*. Dev Biol. 2007; 303:191–201. [PubMed: 17196192]
26. Feng JQ, Ward LM, Liu S, Lu Y, Xie Y, Yuan B, Yu X, Rauch F, Davis SI, Zhang S, Rios H, Drezner MK, Quarles LD, Bonewald LF, White KE. Loss of DMP1 causes rickets and osteomalacia and identifies a role for osteocytes in mineral metabolism. Nat Genet. 2006; 38:1310–1315. [PubMed: 17033621]
27. Luo G, Santoro IM, McDaniel LD, Nishijima I, Mills M, Youssoufian H, Vogel H, Schultz RA, Bradley A. Cancer predisposition caused by elevated mitotic recombination in Bloom mice. Nat Genet. 2000; 26:424–429. [PubMed: 11101838]
28. Kasper D, Planells-Cases R, Fuhrmann JC, Scheel O, Zeitz O, Ruether K, Schmitt A, Poet M, Steinfeld R, Schweizer M, Kornak U, Jentsch TJ. Loss of the chloride channel ClC-7 leads to lysosomal storage disease and neurodegeneration. EMBO J. 2005; 24:1079–1091. [PubMed: 15706348]
29. Katz RW. An analysis of compound and complex odontomas. ASDC J Dent Child. 1989; 56:445–449. [PubMed: 2808859]
30. Wise GE, King GJ. Mechanisms of tooth eruption and orthodontic tooth movement. J Dent Res. 2008; 87:414–434. [PubMed: 18434571]
31. Begg SK, Radley JM, Pollard JW, Chisholm OT, Stanley ER, Bertoncello I. Delayed hematopoietic development in osteopetrotic (op/op) mice. J Exp Med. 1993; 177:237–242. [PubMed: 8418205]
32. Niida S, Kaku M, Amano H, Yoshida H, Kataoka H, Nishikawa S, Tanne K, Maeda N, Nishikawa S, Kodama H. Vascular endothelial growth factor can substitute for macrophage colony-stimulating factor in the support of osteoclastic bone resorption. J Exp Med. 1999; 190:293–298. [PubMed: 10432291]
33. Yoshino M, Yamazaki H, Yoshida H, Niida S, Nishikawa S, Ryoke K, Kunisada T, Hayashi S. Reduction of osteoclasts in a critical embryonic period is essential for inhibition of mouse tooth eruption. J Bone Miner Res. 2003; 18:108–116. [PubMed: 12510811]
34. Fong HK, Foster BL, Popowics TE, Somerman MJ. The crowning achievement: getting to the root of the problem. J Dent Educ. 2005; 69:555–570. [PubMed: 15897336]
35. Tiffee JC, Xing L, Nilsson S, Boyce BF. Dental abnormalities associated with failure of tooth eruption in src knockout and op/op mice. Calcif Tissue Int. 1999; 65:53–58. [PubMed: 10369734]

36. Ida-Yonemochi H, Noda T, Shimokawa H, Saku T. Disturbed tooth eruption in osteopetrotic (op/op) mice: histopathogenesis of tooth malformation and odontomas. J Oral Pathol Med. 2002; 31:361–373. [PubMed: 12201247]

37. Nakajima Y, Shimokawa H, Terai K, Onoue H, Seino Y, Tanaka H, Sobue S, Kitamura Y, Nomura S. Identification of the cell type origin of odontoma-like cell masses in microphthalmic (mi/mi) mice by *in situ* hybridization. Pathol Int. 1996; 46:743–750. [PubMed: 8916143]

38. Dobbins DE, Joe B, Hashiramoto A, Salstrom JL, Dracheva S, Ge L, Wilder RL, Remmers EF. Localization of the mutation responsible for osteopetrosis in the op rat to a 1. 5-cM genetic interval on rat chromosome 10: identification of positional candidate genes by radiation hybrid mapping. J Bone Miner Res. 2002; 17:1761–1767. [PubMed: 12369779]

39. Ogbureke KU, Zhao Q, Li YP. Human osteopetroses and the osteoclast V-H+-ATPase enzyme system. Front Biosci. 2005; 10:2940–2954. [PubMed: 15970548]

40. van der Eerden BC, Hoenderop JG, de Vries TJ, Schoenmaker T, Buurman CJ, Uitterlinden AG, Pols HA, Bindels RJ, van Leeuwen JP. The epithelial Ca2+ channel TRPV5 is essential for proper osteoclastic bone resorption. Proc Natl Acad Sci U S A. 2005; 102:17507–17512. [PubMed: 16291808]

41. Coxon FP, Rogers MJ. The role of prenylated small GTP-binding proteins in the regulation of osteoclast function. Calcif Tissue Int. 2003; 72:80–84. [PubMed: 12370802]

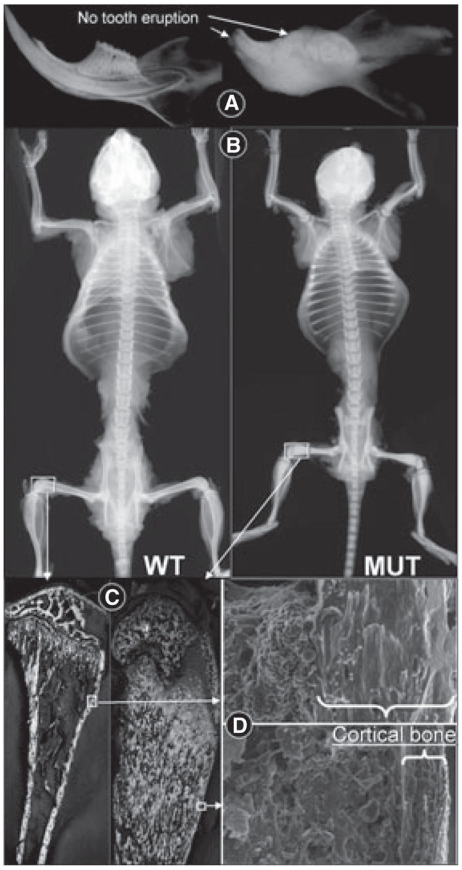

Fig. 1.

The osteopetrosis phenotypes in *ntl* mice. (A) Representative lower jaws of 7-month-old unaffected [wild-type (WT), left panel] and affected [mutant (MUT), right panel] littermates, showing no tooth eruption. (B) Representative whole-body radiograph of 5-wk-old unaffected (WT, left panel) and affected (MUT, right panel) littermates. Note different intensities between the edges and the middle portion of the endochondral elements in the unaffected animal compared with the rather uniform intensity throughout the entire elements in the mutant with little bone marrow spaces. (C) Scanning electron microscope images of a pair of tibiae from these littermates showing the prominent bone marrow space (the dark area) between the cortical bones (in white) from the WT animal compared with the relatively uniform (opaque) appearance in that from the mutant, a characteristic of severe osteopetrosis (right panel). (D) An enlarged portion of areas corresponding to the cortical bones of the same pair of animals in (C) taken on a light box, showing a much thinner cortical bone in the mutant animal (lower panel) compared with that of the WT animal (upper panel).

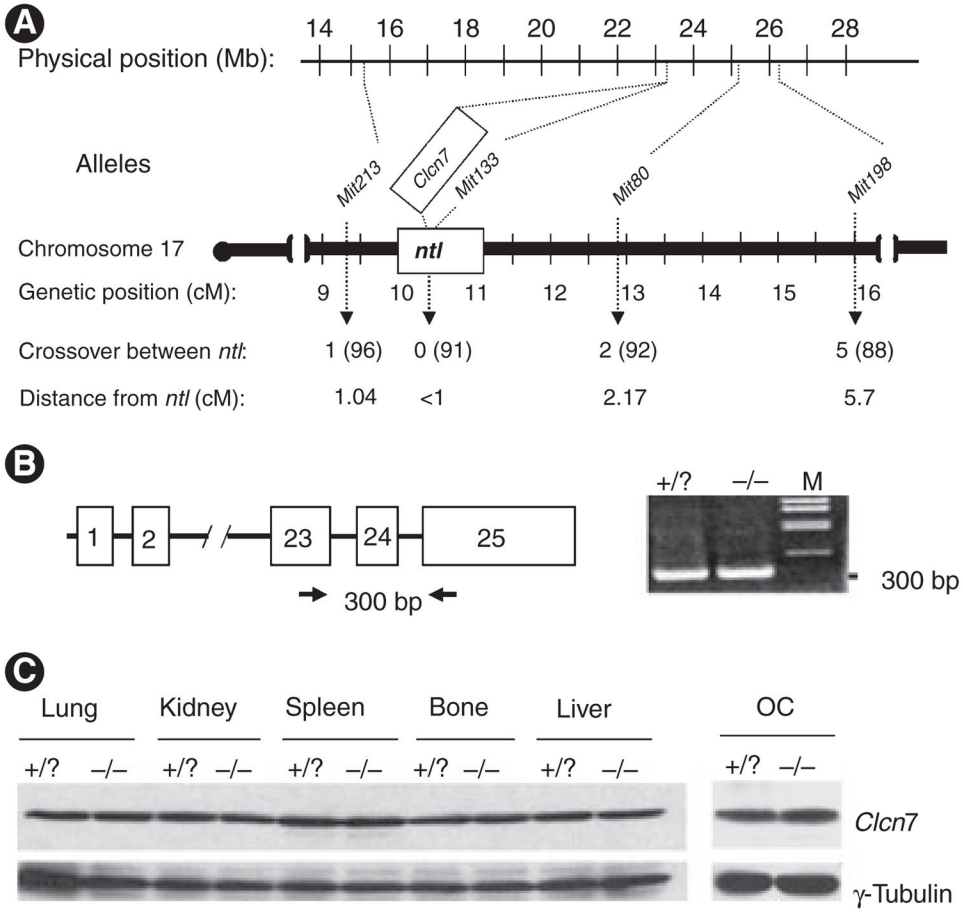

Fig. 2.

Localization of the mutant allele to chromosome 17 and normal expression of Clcn7 in the mutant mice. (A) A schematic diagram summarizing the result of a more extensive genetic linkage analysis for determining the location of the mutant allele on chromosome 17. A map of the genetic interval between 9 and 16 cM of mouse chromosome 17 is shown in the middle. The positions of the *Clcn7* gene (the only known osteopetrosis gene in this region) and the four *Mit* alleles used for the linkage analysis, are indicated below the map; whereas the relative physical positions (Mb) of individual alleles are shown on the top of the map. The result of the linkage analyses is presented as the number of crossovers observed among a defined number of gametes analyzed (in parenthesis). The estimated genetic distances between the mutant allele (*ntl*) and each *Mit* allele are shown at the bottom. Note the lack of any crossover observed between the mutant (*ntl*) allele and the *D17Mit133* allele among 91 gametes analyzed. Also note the discordance between the ratios of the genetic distance/the physical distance on either sides of *D17Mit133*. (B) A representative result of a reverse transcription–polymerase chain reaction (RT-PCR) experiment showing amplification of the *Clcn7* complementary DNA (cDNA) fragment from both unaffected (+/?) and mutant osteoclasts (−/−), because we were not able to distinguish between +/+ and +/− and mutant (−/−) osteoclasts. The positions of the primers (arrows) used to amplify a portion of *Clcn7* cDNA between exons 23 and 25 by RT-PCR, and the expected RT-PCR product (300 bp),

are indicated. M, 1-kb ladder size marker from Invitrogen. (C) Analysis of Clcn7 protein expression by western blotting. The results of western blot experiments using rabbit anti-Clcn7 N-11753 are shown (top panel). Anti-lamin A was used as the control for loading (bottom panel). Note the similar levels of Clcn7 protein expression between the wild-type (+/?) and mutant (−/−) in every type of cell, tissue, or organ examined. OC, osteoclast-enriched cells from cultured splenic cells.

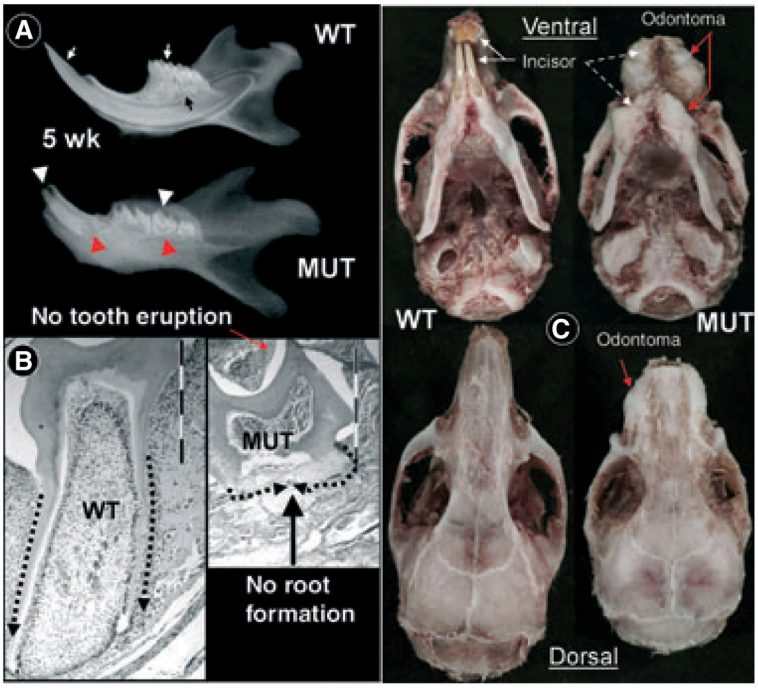

Fig. 3.

Lack of tooth root formation associated with odontoma- like proliferations in the mutant mice. (A) Representative radiographs of whole mandibles in 5-wk-old wild-type (WT, above) and mutant (MUT, below) littermates. Note that the erupted incisor and molars are present in the WT mouse (white arrows) but not in the MUT mouse (black arrowheads). The tooth roots of both incisor and molars are observed in the jaw of the WT mouse (black arrowhead) but absent in the jaw of the mutant mouse (red arrowheads). (B) Tissue sections of the first molars from the WT (left panel) and the MUT (right panel) mice, showing that there is no tooth eruption (red arrow) or root formation (black arrows) in the MUT mouse. (C) Photographs showing the ventral (upper) and dorsal views of the skulls of 7-month-old WT (left) and MUT (right) littermates. Note the odontoma-like proliferations in the mutant (arrows).

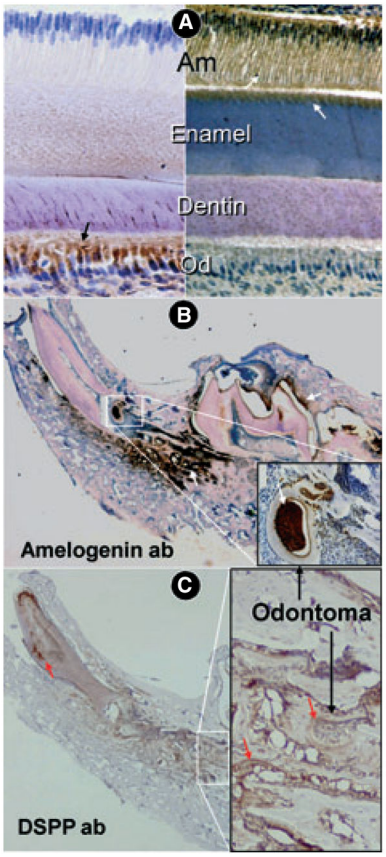

Fig. 4.

Histological images of odontoma-like proliferations in a 7-month-old mutant. (A) Expression of amelogenin in ameloblasts and early enamel (white arrows, right panel), and of dentin sialophosphoprotein (DSPP) in odontoblasts and dentin (black arrow, left panel), in a wild-type mouse. (B) Expression of amelogenin in the odontoma from the mutant mouse (arrows). (C) DSPP expression in the odontoma-like proliferations from the mutant mouse (arrows).

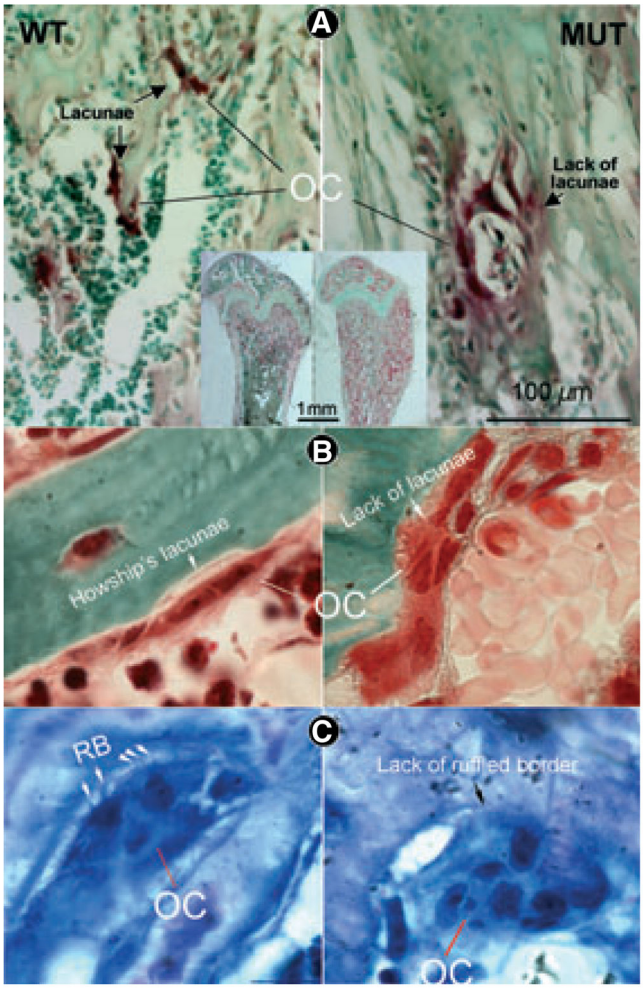

Fig. 5.

Malformed osteoclasts in mutant mice. (A) Tartrate-resistant acid phosphate (TRAP) staining of sections of femurs of 4-wk-old wild-type (WT) (left panel) and mutant (MUT) (right panel) mice were stained for osteoclasts and counter-stained with Methyl Green. Note the presence and absence of bone marrow cavities at the regions of diaphysis in WT and MUT animals, respectively. (B) Goldner's trichrome-stained sections of non-decalcified cancellous bone (green, calcified matrix; red, non-mineralized matrix). Note the prominent Howship's lacunae associated with osteoclasts in the WT mouse (left panel, arrows) but not in the mutant mouse (right panel). (C) Toluidine Blue-stained sections of femur (purple = bone; blue = osteoclasts). Ruffled borders were often observed in osteoclasts from the WT mouse (RB, arrows, left panel) but not in osteoclasts from the MUT mouse (right panel).

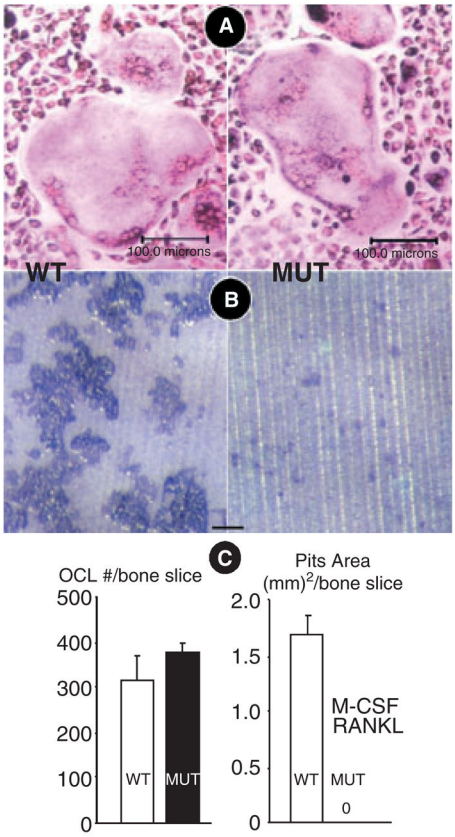

Fig. 6.

Differentiation and bone-resorption activity of cultured *ntl* mutant osteoclasts. (A) Photographs of tartrate-resistant acid phosphate (TRAP)-positive cells derived from *in vitro* cultured splenic cells of wild-type (WT, left) or mutant (MUT, right) mice. (B) Photographs of resorption pits on ivory slice surfaces after incubation with splenic cells from either WT or MUT mice. Note the prominent clusters of resorption pits on the surface of the slice incubated with the WT splenocytes and the absence of such clusters when the slice was incubated with the MUT splenocytes (scale bars equal 100 mm). (C) Quantification of osteoclast numbers per bone slice and pits area. There was no significant difference between the WT and MUT osteoclast numbers in response to macrophage colony-stimulating factor (M-CSF) and receptor activator of nuclear factorκB ligand (RANKL) (left panel, WT; right panel, MUT). Note that there is no pit formation at all in the mutant (MUT, right panel). OCL, osteoclast. The y-axis in the left and the right panel denotes the number of osteoclast and the area with resorption pits per area, respectively.

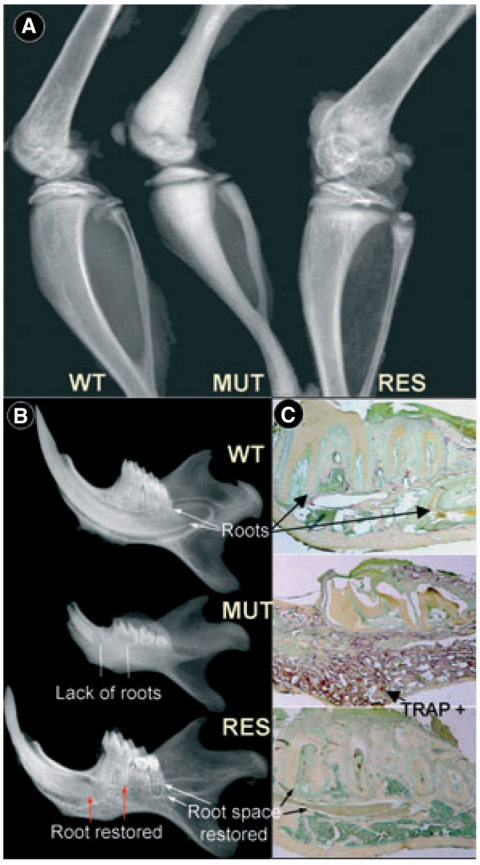

Fig. 7.

Rescue of the mutant (MUT) phenotype by injections of osteoclast progenitor cells into the MUT mice. (A) Radiographs of hindlimbs from an unaffected wild-type (WT) mouse, a MUT mouse, and a MUT mouse that was injected with progenitor cells from WT fetal liver cells after irradiation (rescued, RES) at the age of 4 wk. (B) Radiographs of mandibles from the same littermates: WT, MUT, and RES. (C) Tartrate-resistant acid phosphate (TRAP)-stained mandibles from the same littermates: WT, MUT, and RES. Note that there are few TRAP-positive stained osteoclasts in the WT (upper panel) and the RES (lower panel) groups compared with the MUT (middle panel), suggesting a restoration of normal osteoclastogenesis in the rescued mutant.

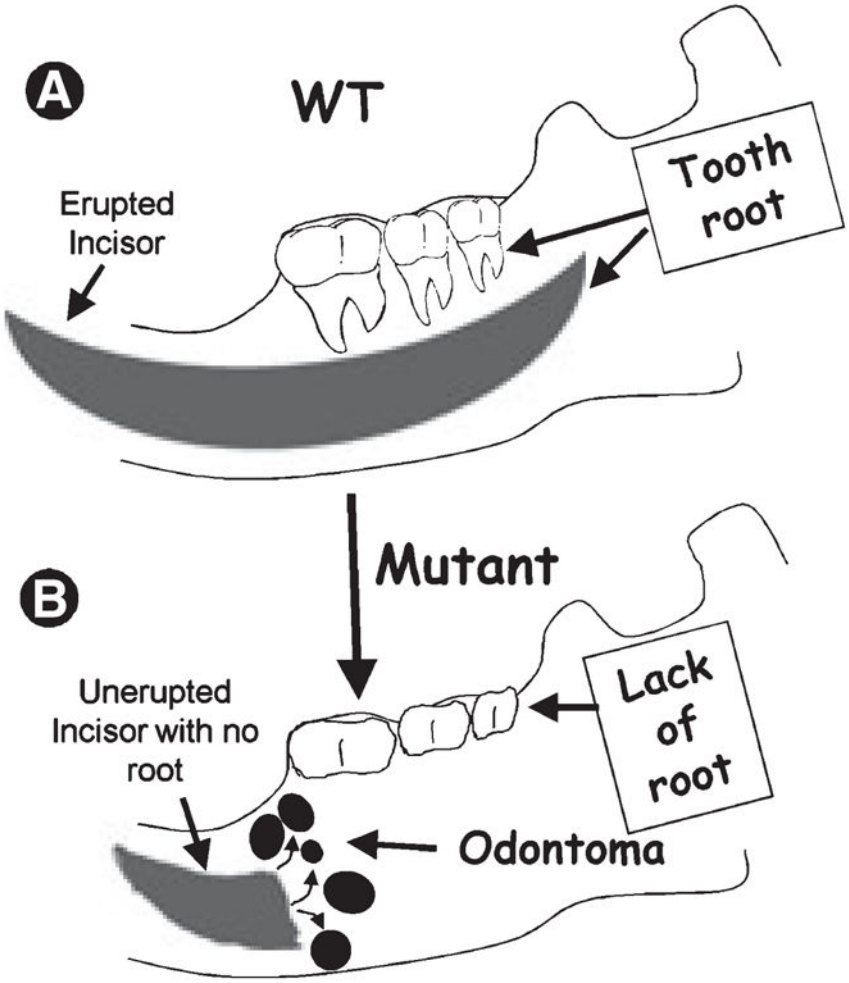

Fig. 8.

Working hypothesis: osteoclast-mediated bone resorption is required for formation of the tooth root space in the central spongiosa where the tooth root will be held (A). Defects in osteoclasts result in the absence of bone spaces for the tooth root to grow in, leading to the absence of the tooth root. The rodent incisor grows continuously throughout life, whereas the molar does not. As a result, the odontoma-like proliferations probably derive from continuous differentiation of dental and enamel stem cells in the proximal mutant incisor (B).

Table 1

Segregation of the ntl mutant allele with Mit alleles linked to osteopetrosis genes

Osteopetrosis gene	Linked *Mit* allele	Genetic distance (cM)*	Percentage homozygosity in *ntl* mutant mice†	Sample size‡
Gl	*D10Mit38*	1.3	55	40
Clcn7	*D17Mit198*	6.0	95	42
Atp6i	*D19Mit41*	10.0	52	41
c-Src	*D9Mit156*	10.0	48	39

*Genetic distance between individual known osteopetrosis genes and linked *Mit* alleles.

†If a tested *Mit* allele is linked to the *ntl* allele, they are expected to cosegregate at a frequency proportional to the distance between them. However, if they are not linked, they are expected to segregate independently and therefore the expected frequency of homozygosity of the *Mit* allele among homozygous *ntl* mutants is expected to be approximately 50%.

‡The total number of informative gametes analyzed for the particular *Mit* allele.